

## Controlling the exchange bias field in Co core/CoO shell nanoparticles

Mikhail Feyngenson,<sup>1</sup> Yuen Yiu,<sup>1</sup> Angela Kou,<sup>1</sup> Ki-Sub Kim,<sup>2</sup> and Meigan C. Aronson<sup>1,3,\*</sup>

<sup>1</sup>Condensed Matter Physics and Materials Science Department, Brookhaven National Laboratory, Upton, New York 11973-5000, USA

<sup>2</sup>Department of Chemical and Biological Engineering, Chungju National University, 72 Daehak-ro, Chungju, Chungbuk 380-702, Korea

<sup>3</sup>Department of Physics and Astronomy, Stony Brook University, Stony Brook, New York 11794, USA

(Received 19 February 2010; revised manuscript received 16 April 2010; published 28 May 2010)

We have determined how the anomalous exchange bias effect in Co/CoO nanoparticles of 11 nm in diameter depends on the Co core and CoO shell dimensions. The oxidation of the Co nanoparticles used in this study is carefully controlled, yielding highly crystalline and oriented interfaces. The dimensions of the core and shell are determined from magnetization and small angle x-ray scattering measurements. The exchange bias field in Co/CoO core-shell nanoparticles depends nonmonotonically on the CoO shell thickness, reaching a maximum value of  $\approx 7$  kOe at 30 K when the core and shell dimensions are similar. We propose that lattice strain induces a net moment at the core-shell interface, and it is the variation of this moment with strain, which is responsible for the vanishing of  $H_{EB}$  at both large and small Co shell thicknesses.

DOI: [10.1103/PhysRevB.81.195445](https://doi.org/10.1103/PhysRevB.81.195445)

PACS number(s): 81.07.-b, 73.22.Dj, 75.60.-d

### I. INTRODUCTION

The exchange bias effect occurs when a ferromagnet (FM) in direct contact with an antiferromagnet (AFM) is cooled below the Néel temperature of the latter in an applied magnetic field. If the AFM anisotropy  $K_{AFM}$  is strong enough, the magnetization loop of such a system is shifted along the field axis by the exchange bias field  $H_{EB}$ .<sup>1</sup> The exchange bias effect in magnetic nanostructures remains one of the most intensively studied topics in condensed matter physics,<sup>1-3</sup> in part because it is a promising way to stabilize small ferromagnetic particles against thermal fluctuations,<sup>3,4</sup> potentially providing a route to higher density magnetic recording. However, a fundamental understanding of the exchange bias effect remains incomplete.<sup>3</sup> A key consideration for the design of magnetic devices is to specify the relative dimensions of the ferromagnet and antiferromagnet, which maximize the exchange bias field. Previous experiments on thin films found that  $H_{EB} \sim 1/t_{FM}$ , which as ascribed to negligible FM anisotropy and strong coupling at the AFM-FM interface.<sup>3,5-11</sup> The dependence of  $H_{EB}$  on the thickness of the AFM has been less studied, although the general trend suggests that this relationship is nonmonotonic.<sup>12-16</sup> These studies have all been impacted to differing extents by extrinsic factors, such as domain formation, interfacial roughness, impurities, and grain boundaries, all of which affect the exchange bias effect in nontrivial and somewhat uncontrollable ways.<sup>9,11,17,18</sup> Many of these factors can be more readily controlled in nanoparticle systems, where low-temperature syntheses can result in nanocomposite systems where the ferromagnetic core and antiferromagnetic shell are highly crystalline, and their interface nearly epitaxial in quality.<sup>19</sup> In several of these systems, the exchange bias field approaches the values estimated by simple theories,<sup>15,19-21</sup> indicating that the complications of extrinsic effects can potentially be overcome.

Establishing how the exchange bias field depends on the dimensions of the ferromagnetic and antiferromagnetic components of a nanoparticle system has proven to be a signifi-

cant technical challenge, as previous experiments have shown. First, all parts of the nanoparticle must be highly crystalline, but especially in the vicinity of the AFM-FM interface.<sup>3,5</sup> Both the ferromagnetic and antiferromagnetic components must also be single domain.<sup>2</sup> Finally, the synthesis process must produce nanoparticles with controllable and monodispersed AFM and FM dimensions, which must be accurately measured.<sup>15,22</sup> We present here the results of our measurements of the exchange bias effect in highly crystalline Co core/CoO shell nanoparticles, where the samples represent different stages of oxidation of the same preparation batch. We will use a combination of magnetization and small angle x-ray scattering (SAXS) experiments to accurately determine the core and shell dimensions, and demonstrate that interparticle interactions play no appreciable role in the magnetic processes, including the exchange bias effect. Our results confirm and expand initial reports that the exchange bias field  $H_{EB}$  depends nonmonotonically on the ferromagnetic core diameter.<sup>15,21</sup> By appealing to neutron diffraction experiments carried out on similar samples,<sup>19</sup> we argue that variations in the strain induced coupling of the core and shell are responsible for this effect.

### II. SAMPLES AND EXPERIMENTS

Co nanoparticles are prepared by the thermal decomposition of  $\text{Co}_2(\text{CO})_8$  in hot oleic acid as described in Ref. 23. Once the particles have fully formed, we oxidize the Co nanoparticles *in situ* by bubbling oxygen through the suspension at 180 °C, and take aliquots of the oxidizing particles after 25, 50, 90, 140, and 295 min have elapsed. We obtain six samples in total (M1–M6), including a reference sample of the unoxidized Co nanoparticles (M1). We then wash the nanoparticles in ethanol to remove excess oleic acid, and redisperse them in paraffin for magnetization measurements and toluene for SAXS measurements. Transmission electron microscope (TEM) measurements show that the Co particles which we will use for our study have an unoxidized diameter of  $11 \pm 2$  nm, a polydispersivity typical of this synthesis

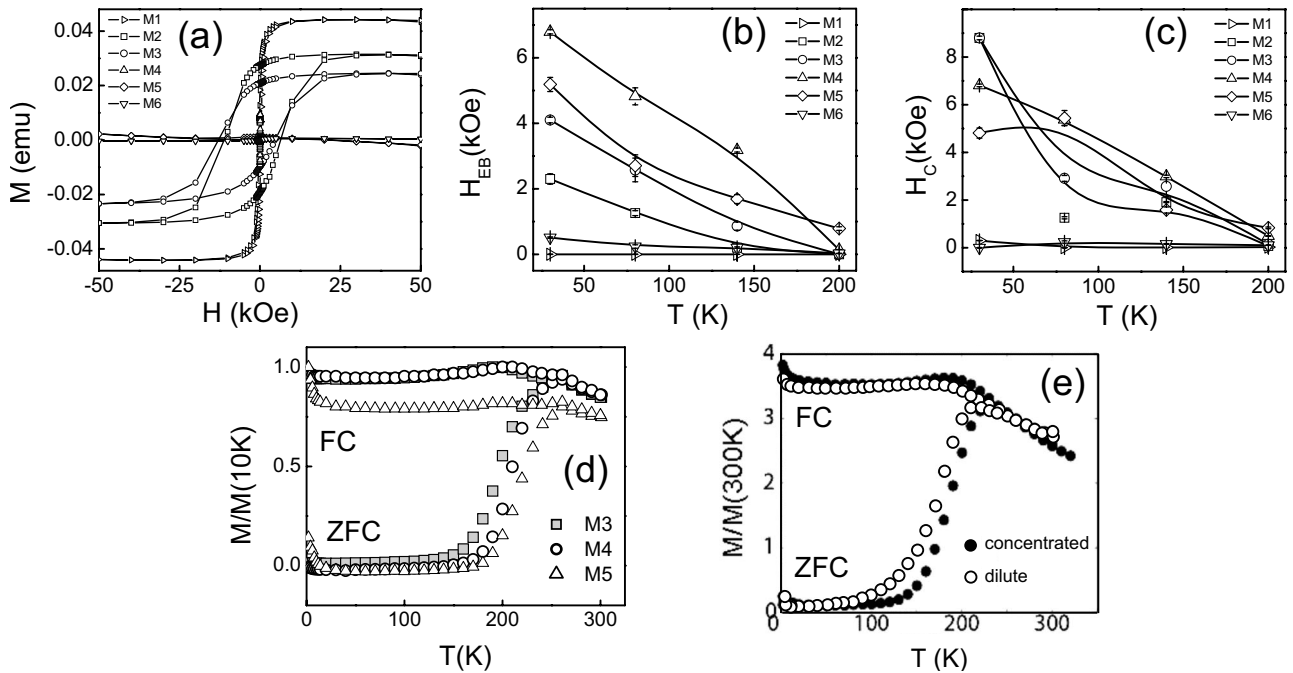


FIG. 1. (a) Field dependent magnetizations of six samples of Co core/CoO shell nanoparticles, measured at 30 K. (b) The temperature dependence of the exchange bias field  $H_{EB}$  for all six samples. Solid lines are guides for the eye. (c) Temperature dependence of the coercive field  $H_C$  for the same six samples. (d) The temperature dependent magnetization  $M(T)$  normalized to the highest field-cooled value  $M_{10\text{ K}}$  for samples M3, M4, and M5. (e) A comparison of the temperature-dependent magnetizations for dilute and concentrated powders of Co/CoO nanoparticles.

procedure.<sup>19,23</sup> Since oxidation occurs at relatively low temperature and while the particles are in suspension, the CoO shell forms relatively slowly but uniformly on each particle. This results in a near-epitaxial core-shell interface that is oriented along the CoO (100) and equivalent crystal directions. Unlike oxidation studies which are done on precipitated ferromagnetic particles, our procedure yields core-shell particles with highly uniform CoO shell thicknesses, likely reflecting the oxygen diffusion length itself. We note that the dual effect of the oxide coating and the attachment of oleic acid to the individual particles greatly inhibits agglomeration when the particles are precipitated from solution, unlike the case of strongly ferromagnetic particles.

Magnetization measurements were carried out using a quantum design magnetic property measurement system (MPMS). 10  $\mu\text{l}$  of the original aliquots was dispersed in 50  $\mu\text{l}$  of liquid paraffin and then injected into a standard gelatin capsule. In order to measure the exchange bias field, a sample is cooled from 300 to 30 K in an applied magnetic field of 50 kOe. The magnetization is then measured as a function of an applied magnetic field at 30, 80, 140, and 200 K. The exchange bias field  $H_{EB}$  is determined from the loop shift after subtracting the linear diamagnetic magnetization of paraffin. The exchange bias field is calculated as  $H_{EB} = |H_{c1} - H_{c2}|/2$ , where  $H_{c1}$  and  $H_{c2}$  are the negative and positive coercive fields, respectively. The temperature-dependent magnetization  $M(T)$  was measured in a fixed field of 500 Oe.

SAXS measurements were performed at the X-21 beamline at the National Synchrotron Light Source at Brookhaven National Laboratory. About 10 mg of each original aliquot is suspended in 200  $\mu\text{l}$  of toluene and injected into quartz cap-

illaries with 1 mm thick walls. We further diluted the underoxidized samples M2–M3 and nonoxidized sample M1 by a factor of 20 to reduce possible interparticle interactions, which may otherwise be present because of the dipole-dipole interactions between Co cores, which we will discuss below. All samples were measured at the same x-ray wavelength of 1.24  $\text{\AA}$ . The data are corrected for background scattering from the quartz capillary and toluene, as well as for beam attenuation.

### III. RESULTS

Figure 1(a) shows the full-magnetization loop  $M(H)$  after cooling from room temperature in a field of 50 kOe. The oxidized samples demonstrate a substantial shift of the loop toward negative fields, while no shift is observed for the bare Co nanoparticles under the same experimental conditions. We have plotted the temperature dependencies  $H_{EB}(T)$  in Fig. 1(b), and the values of  $H_{EB}$  for each of the six samples are summarized in Table I. We see that  $H_{EB}$  first becomes nonzero at  $\approx 200$  K in each sample and increases with decreasing temperature. In the first stages of oxidation (M1)  $H_{EB}$  is very small, but initially increases rapidly at all temperatures with increasing oxidation (M2, M3, and M4). Maximum values for  $H_{EB}$  approaching 7 kOe are found in samples M4 and M5, similar to values found by us and by others in previous measurements on differently sized Co core/CoO shell nanoparticles,<sup>4,15,19,20</sup> although somewhat larger values have been reported for Co/CoO bilayer samples.<sup>24–26</sup> Further oxidation (M6) leads to a strong reduction in  $H_{EB}(T)$ , until it is only slightly larger than that of the

TABLE I. Samples obtained by the progressive oxidation of a single batch of Co nanoparticles. Here  $\tau$  is the oxidation time,  $R$  is the radius of the Co core and  $t$  the thickness of the CoO shell. The subscript identifies the technique used to determine the dimensions:  $M$  is magnetization measurements, SAXS is the small angle x-ray scattering.  $H_{EB}$  is the maximum of the exchange biased field observed at 30 K after field cooling in 50 kOe from room temperature.

Sample	$\tau$ (min)	$R_M$ (nm)	$t_M$ (nm)	$R_{SAXS}$ (nm)	$t_{SAXS}$ (nm)	$H_{EB}$ (kOe)
M1	0	5.60(0.54)	0.00(0.14)	3.20(0.61)	1.20(0.49)	0
M2	25	4.97(0.49)	0.63(0.14)	3.50(0.66)	1.00(0.60)	2.30(0.16)
M3	50	4.58(0.46)	1.02(0.13)	3.50(0.62)	0.98(0.60)	4.10(0.086)
M4	90	3.19(0.31)	2.41(0.12)	2.25(0.42)	2.61(0.31)	6.79(0.63)
M5	140	1.39(0.16)	4.21(0.11)	1.46(0.27)	3.70(0.11)	5.18(0.22)
M6	295	1.05(0.14)	4.55(0.11)	0.50(0.11)	4.60(0.46)	0.52(0.019)

nominally unoxidized sample M1. A similar trend with oxidation was observed for the coercive field  $H_C(T)$  (Fig. 1(c)). No vertical shifts of the magnetization loops were found in any of our samples, at any temperature. This indicates that there are relatively few uncompensated spins in our samples.<sup>27,28</sup>

Figure 1(a) also demonstrates a monotonic decrease of the saturation magnetization  $M_S$  as the oxidation time increases. Since the overall diameter and concentration of the Co/CoO nanoparticles is the same for each sample M1–M6, we ascribe the decrease in the saturation magnetization to the decrease of the Co core radius as the antiferromagnetic CoO shell becomes progressively thicker. By normalizing the measured magnetization of each sample to the value measured in the bare Co nanoparticles, we can calculate the volume of the Co core and thus infer the volume of the CoO shell in each sample. The calculated values for the radius of the core  $R_M$  and the thickness of the shell  $t_M$  are also presented in Table I. Using the standard value of 162 emu/g for Co<sup>29</sup> and taking the particle diameter from TEM and SAXS measurements to be 11 nm, we deduce that each sample consists of about  $4 \times 10^{16}$  nanoparticles.

The temperature-dependent magnetization reveals that the blocking temperature  $T_B \approx 200$  K for all samples, independent of the Co core and CoO shell dimensions, except for the M5 sample, where  $T_B$  appears to be slightly higher [Fig. 1(b)]. This indicates that the superparamagnetic dynamics of the Co core, which dominate the response at higher temperatures are frozen out below  $\approx 200$  K, where core reversal and reorientation are controlled by an energy barrier which is dominated by the exchange energy of interaction between the ferromagnetic core and the antiferromagnetic shell, and not by a volume dependent energy barrier  $KV$  due to magnetocrystalline anisotropy.<sup>30</sup> Interactions between particles can affect both the blocking temperature and the magnitude of the exchange bias effect in some systems.<sup>31–33</sup> To test this possibility, we have measured  $M(T)$  for another sample of Co core/CoO shell nanoparticles, this time with an overall particle diameter of 7 nm [Fig. 1(e)]. No appreciable difference is observed in the blocking temperature for the precipitated powder, where the particles are approximately 1 diameter apart, and a dilute suspension in paraffin, where the average separation among the particles is  $\approx 5$  particle diam-

eters. The same value of the exchange bias field is observed in both samples after field cooling in a 50 kOe field. We conclude that interparticle interactions have no measurable effect on the dynamical blocking of our samples.

SAXS experiments are used to provide independent measurements of the dimensions of the particle cores and shells, and to test for the possible presence of agglomeration in our samples. Measurements of the SAXS intensity for each of the samples M1–M6 are plotted as functions of the scattering vector  $q$  in Fig. 2. In each case, the measurements were performed at room temperature. The data are fitted using software which was originally developed for small angle neutron scattering measurements at the NIST Center for Neutron Research,<sup>34</sup> adapted here for the analysis of SAXS data by converting electron densities into neutron scattering length densities. The  $q$  dependence of the SAXS intensity  $I(q)$  is fitted using a combination of two models. The first model uses a form factor of spherical core-shell nanoparticles assuming a polydispersed core and monodispersed shell.<sup>35</sup> We believe this assumption is appropriate, since our transmission electron microscopy studies of similar Co core/CoO shell nanoparticle samples<sup>19</sup> indicate that the CoO shell thickness is virtually identical in each particle, and is pre-

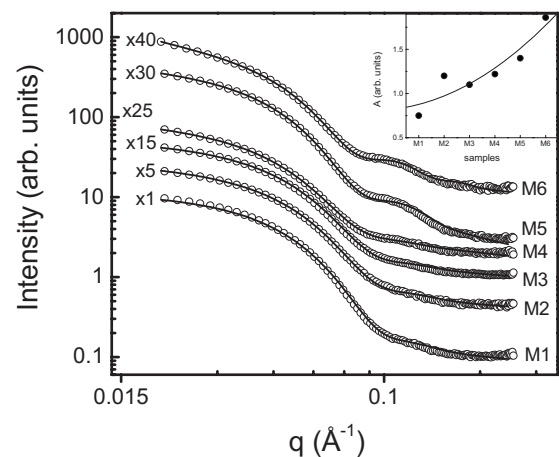


FIG. 2. Log-log plot of the scattered x-ray intensity measured as a function of scattering vector  $q$  at room temperature (open circles) and fits to the model described in the text (solid lines). Inset: the power law coefficient  $A$  for different samples.

TABLE II. The parameters determined by fitting SAXS data taken on sample M2.  $c$  is the overall intensity scale parameter;  $R_{\text{SAXS}}$  is the radius of the Co core;  $\Delta R_{\text{SAXS}}$  is the core polydispersivity;  $t_{\text{SAXS}}$  is the thickness of the CoO shell, and  $\rho_{\text{core}}$ ,  $\rho_{\text{shell}}$ , and  $\rho_{\text{solv.}}$  are the scattering length densities for the Co core, CoO shell and toluene, respectively;  $A$ ,  $B$  and  $bk g$  are the parameters of the power law  $I(q) = Bq^{-A} + bk g$ .

Parameter	Average value	Standard deviation
$c$	$5.58 \times 10^{-5}$	Fixed
$R_{\text{SAXS}}$ (nm)	3.50	0.66
$\Delta R_{\text{SAXS}}$	0.19	$3.00 \times 10^{-3}$
$t_{\text{SAXS}}$ (nm)	4.72	0.20
$\rho_{\text{core}}$ ( $\text{\AA}^{-2}$ )	$6.92 \times 10^{-5}$	Fixed
$\rho_{\text{shell}}$ ( $\text{\AA}^{-2}$ )	$4.62 \times 10^{-5}$	Fixed
$\rho_{\text{solv.}}$ ( $\text{\AA}^{-2}$ )	$8.40 \times 10^{-6}$	Fixed
$B$ (a.u.)	$1.60 \times 10^{-3}$	$4.10 \times 10^{-5}$
$A$ (a.u.)	-1.20	0.25
$bk g$ ( $\text{cm}^{-1}$ )	0.02	Fixed

sumed to reflect the finite diffusion length of oxygen at the oxidation temperature of 180 °C. In this way, all polydispersivity can be associated with the overall particle diameter and hence, that of the Co core. The second model is the power law superposed on a  $q$ -independent background  $I(q) = Bq^{-A} + bk g$ , which describes the formation of chainlike aggregates, resulting in the nonsaturating behavior of the scattered intensity  $I(q)$  at low  $q$ . The formation of chainlike structures has been previously reported in a SAXS experiment carried out in a suspension of similarly sized Co nanoparticles.<sup>36</sup> During the fitting we fix the scattering length densities of the Co, CoO, and toluene to their bulk values in order to reduce the number of free parameters.<sup>37</sup> The best fits for all samples are represented by the solid lines in Fig. 2. We believe that modest discrepancies between the data and the fits, evident particularly in the most heavily oxidized samples at higher  $q$ , may be due to a reduced density of the Co and possibly the CoO caused by finite size effects.<sup>38,39</sup> A representative set of fitting parameters determined from the SAXS experiment on the M2 sample is presented in Table II.

We have added the core radius  $R_{\text{SAXS}}$  and the shell thickness  $t_{\text{SAXS}}$ , which were determined from the SAXS fitting parameters to Table I. The SAXS measurement finds that the core radius and the particle diameter have  $\approx 10\%$  polydispersivity, although slightly larger values are found in M5 and M6. We see that the core and shell dimensions determined from the SAXS measurements are in reasonable agreement with the values determined from magnetization measurements, previously described. Because nanoparticles in toluene are more vulnerable to oxidation than nanoparticles in paraffin, we attribute the slight differences between the two measurements in the core and shell dimensions to additional oxidation of the Co/CoO nanoparticles during the SAXS measurements. This effect is especially pronounced in the nominally bare Co nanoparticles (sample M1). While magnetization measurements show zero exchange bias field in sample M1, consistent with the absence or near absence of a

CoO shell, the SAXS measurements indicate that for the same sample dispersed in toluene a CoO shell of 1.2 nm has formed. We must conclude that the CoO overlayer revealed by the SAXS measurements is below the critical thickness required to enable a measurable exchange bias effect.<sup>40</sup>

The fits to the SAXS data indicate that residual dipolar interactions among particles, while not appreciably affecting the magnetization dynamics at room temperature, lead to the formation of structures with length scales which are longer than the particle diameters themselves. The inset of Fig. 2 indicates an increase of the power law exponent  $A$  with increasing degree of oxidation in our samples. The implication is that oxidation reduces the size of the Co core and since the cores are always prevented from closer contact by the attached surfactant and the surrounding CoO shells, we must conclude that the dipolar interactions among the particles are weak. In slightly oxidized samples, the value of  $A$  is small, indicating that the dipolar interactions arrange the core/shell particles into chainlike structures. In the more highly oxidized samples, the interactions are weaker, and the increased value of  $A$  indicates that the chainlike structures are broken down into more complicated, and perhaps less ordered, fractal-like structures.<sup>41,42</sup>

#### IV. DISCUSSION

Using a combination of two independent techniques, magnetization measurements and SAXS, we have determined the core and shell dimensions of Co nanoparticles, which have been progressively oxidized. While the SAXS measurements show some indication of spatial organization of the particles, dilution measurements show that interparticle interactions have no measurable impact on the blocking temperature and the exchange bias field  $H_{\text{EB}}$ . The Co cores in our particles are always too small to sustain multiple ferromagnetic domains.<sup>43</sup> High-resolution transmission electron microscopy (HRTEM) measurements show that our technique of low temperature, in-solution oxidation results in highly oriented interfaces between the Co core and the CoO shell,<sup>19</sup> largely free of the surface roughness and subsequent decomposition of the net interface moment which dominates the interfaces of thin films. It is fair to say that we have demonstrated sufficient control over the properties of our samples to mount a definitive study of how  $H_{\text{EB}}$  depends on the relative dimensions of the ferromagnetic Co core and the anti-ferromagnetic CoO shell.

Our primary result is presented in Fig. 3(a), where we have plotted the values of  $H_{\text{EB}}$ , measured at different fixed temperatures, as a function of the inverse of the Co core radius  $R$ , taken as the average of the values of  $R_M$  and  $R_{\text{SAXS}}$  (Table I). As previously noted,  $H_{\text{EB}}$  increases with decreasing temperature for all samples. Strikingly, Fig. 3(a) shows that  $H_{\text{EB}}$  is small both when the core is small and also when it is large.  $H_{\text{EB}}$  is maximized in sample M4, distinct from the underoxidized samples M1, M2, and M3 where the core is much larger than the shell, and the overoxidized samples M5 and M6 where the shell is much larger than the core. Apparently, a substantial core and a sizable shell are both necessary ingredients for realizing a large value for  $H_{\text{EB}}$ . Importantly,



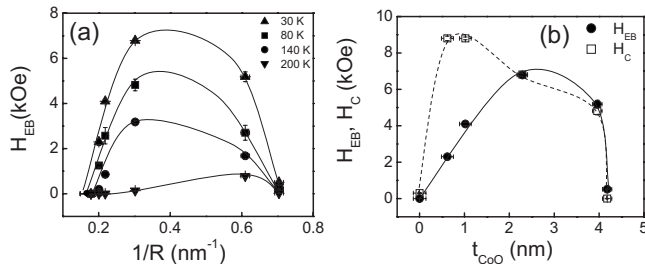


FIG. 3. (a) The exchange bias field  $H_{EB}$  as a function of inverse Co core radius  $R$ . (b) A comparison of  $H_{EB}$  and the coercive field  $H_C$  at 30 K as functions of the CoO shell thickness  $t_{CoO}$ . Solid lines are guides for the eye.

the value of  $H_{EB}$  depends only weakly on the core and shell dimensions in the samples M4 and M5, which have comparable values of  $H_{EB}$  although the core radius of sample M4 is  $\approx 2$  times bigger than that in sample M5. These results are in dramatic conflict with those found in Co/CoO thin films,<sup>3,6–8</sup> which confirm the simplest models of the exchange bias effect, which have  $H_{EB}$  inversely proportional to the thickness of the ferromagnet.<sup>1</sup> Of course, it is worth noting that in the thin film systems, the antiferromagnet is taken as having indefinite lateral size. This is clearly not the case in nanoparticle samples, where we can expect that the magnetic structure can be strongly altered in the vicinity of the core-shell interface and where artificial limits are imposed on both FM and AFM thicknesses.<sup>2,19,44,45</sup> In the current study, the Co core radius and the CoO shell thickness must sum to 5.5 nm, so they are in no way independent variables. This is confirmed when we plot the value of the exchange bias field at 30 K as a function of the CoO shell thickness in Fig. 3(b), showing that the exchange bias is small when the CoO shell is thin (Co core is large) as well as when the CoO shell is thick (Co core is small). A similar trend is observed for the coercive field  $H_C$ , which seems to peak at smaller values of  $t_{CoO}$  than  $H_{EB}$ .

The nonmonotonic behavior of the exchange bias field on the core or shell dimensions is intuitively reasonable. We do not expect an exchange bias effect when the CoO shell is vanishingly small or conversely when the Co core disappears. In both cases,  $H_{EB}$  should approach zero, as it does in Figs. 3(a) and 3(b). It is a more complex issue to understand how  $H_{EB}$  is jointly controlled by the dual influences of an antiferromagnetic shell, which increases in thickness and a ferromagnetic core which at the same time decreases in thickness. The nonmonotonic dependence of  $H_{EB}$  on the antiferromagnetic shell thickness has been previously observed in Co/CoO clusters and nanoparticles, although the core and shell dimensions were not constrained in these experiments.<sup>15,46</sup> It was argued that the initial increase of  $H_{EB}$  with CoO thickness was a finite size effect. Specifically, the Néel temperature  $T_N$  of the CoO shell approaches the bulk value of 293 K when the thickness of the CoO shell is larger than 10 nm, but drops off rapidly with decreasing CoO thickness and reaches values as low as 10 K in CoO nanoparticles with diameters of 1.5 nm.<sup>22,30,47</sup> A nonzero exchange bias field can only be observed when the measurement temperature is smaller than the Néel temperature of the

CoO shell,<sup>48,49</sup> so the apparent increase in  $H_{EB}$  with  $t_{CoO}$  suggests that  $T_N$  passes through a given measurement temperature as the CoO shell exceeds a certain thickness  $t_{CoO}$ . However, we can reject this explanation in our samples. We have directly measured the antiferromagnetic order parameter in similar Co/CoO core-shell nanoparticles using neutron diffraction.<sup>19</sup> Consistent with the uniform onset of the exchange bias effect below a blocking temperature  $T_B \approx 200$  K [Fig. 1(b)], we found that  $T_N \approx 235$  K, independent of core and shell dimensions.

It is entirely possible that part of the variation of  $H_{EB}$  with the decreasing core diameter found in the early stages of oxidation may arise from the same energetics that leads to  $H_{EB} \propto 1/t_{FM}$  in thin film systems,<sup>1</sup> but it is clear that this is not enough to explain the nonmonotonic dependence of  $H_{EB}$  on the dimensions of the nanoparticle core and shell. We propose here that the magnitude of the moment induced by directional lattice strain at the core-shell interfaces plays a crucial role in determining the relationship between  $H_{EB}$  and the core and shell dimensions. Neutron diffraction measurements on similar Co core/CoO shell nanoparticles<sup>19</sup> indicate that the epitaxial growth of CoO on Co leads to a tetragonal strain at the interface, present in both the paramagnetic and antiferromagnetic phases, and with a magnitude that is much larger than that found in bulk CoO.<sup>50–53</sup> This strain is largest in the thinnest CoO layers, relaxes as the oxide layer grows, and ultimately increases again at the highest oxide thickness, presumably as the result of defects introduced during over oxidation. Since the Co-CoO interface is highly directional in our samples, with the interfaces lying along the CoO 100 and equivalent directions, the consequence of the lattice strain on the magnetic structure is profound. The modulation of the antiferromagnetic magnetization in both bulk and nanocrystalline CoO involves two wave vectors,  $q_1 = \frac{2\pi}{a}(\frac{1}{2}, \frac{1}{2}, \frac{1}{2})$ , and  $q_2 = \frac{2\pi}{a}(1, 0, 0)$ .<sup>19</sup> The amplitude of the trigonal  $q_1$  modulation is small and very similar in magnitude in bulk CoO and in the core-shell nanoparticles. However, the amplitude of the tetragonal component with wave vector  $q_2$  is much larger in the core-shell nanoparticles than in bulk CoO, and varies strongly with the CoO thickness, due to unrelaxed tetragonal strains arising from lattice mismatch at the Co-CoO interface. By itself, the  $q_1$  modulation would lead to an antiferromagnetic structure where the moments are perpendicular to the (111) planes, and to the complete moment compensation of the (100) plane. Similarly, the  $q_2$  distortion would lead to antiferromagnetic order where alternating ferromagnetic (100) planes are stacked along the [100] axis, leading to (100) planes that are completely uncompensated. Increasing the  $q_2$  component results in a canting of the interface moments away from the  $q_1$  direction, and to the progressive decompensation of the (100) interface planes.

In underoxidized particles where the CoO shell is very thin (M1, M2, and M3), the strain and hence this canting is at a maximum. We infer that little, if any, of the CoO shell has the undistorted and fully compensated bulk CoO magnetic structure, and that the moment induced at the interface leads to enhanced coupling to the core. No exchange bias effect is expected if the moments in the core and shell reorient together. Lattice strain is found to be less severe in the mod-

erately oxidized particles (M4), and there is less moment canting at the interface. We hypothesize that the moments in the parts of the shell far from the interface return to the compensated magnetic structure of bulk CoO, and are essentially uncoupled from the external field and from the core moments. This situation is exactly what is needed for an optimal exchange bias: there are still strain-induced moments at the interface which enhance the core-shell coupling,<sup>19,54,55</sup> but these moments are impeded from free rotation with the core moments by their exchange interactions with the moments in the outer shell. Increasing the thickness of the CoO shell leads to a further reduction of the interface moment, and now virtually the entire CoO shell approaches the compensated structure of bulk CoO. As was demonstrated in thin film experiments,<sup>56</sup> the observation of an exchange bias effect for ferromagnets exchange coupled to CoO requires an uncompensated interface, and not the nearly compensated (100) interface which is regained in samples M5 and M6, with the thickest CoO shells and the most relaxed interface strains. Finally, we note that the development of the core-shell exchange coupling during the early stages of this process are in at least qualitative agreement with a recent model of the energetics of the exchange bias effect.<sup>40</sup>

## V. CONCLUSION

The possibility of using magnetic core-shell nanoparticles as a storage medium for magnetic recording is appealing, particularly when the moment can be stabilized by the exchange bias effect. Understanding how to optimize the exchange bias effect by varying the dimensions of the core and shell is an important but still unresolved issue which underlies this application. While we concede that the particles used in nanoparticle devices may ultimately be significantly less perfect than those studied here, it is necessary to demonstrate a great deal of control over the particles themselves in order to establish unambiguously how the core and shell dimensions optimize the exchange bias field  $H_{EB}$ . We have used a solution growth technique to create Co particles which are highly crystalline, and with highly monodispersed diameters. These particles are oxidized at low temperatures while they are still in solution, leading to very uniform CoO shell thick-

nesses, with core-shell interfaces which have been shown to be both highly directional and highly ordered. We have taken samples from different stages of this oxidation process, an approach which guarantees that the particle diameter remains constant, while the CoO shell grows thicker just as the Co core becomes smaller. We have used SAXS measurements to directly determine the core and shell dimensions of a much larger assemblage of particles than is possible using transmission electron microscopy measurements. The SAXS measurements also confirm that the interactions among particles in solution are weak, although magnetization measurements carried out for different average particle spacings indicate that interparticle interactions have little impact on the magnetic properties of these core-shell particles. We find that the exchange bias field depends nonmonotonically on the CoO shell thickness, and that the largest values for  $H_{EB}$  approach simple theoretical estimates<sup>15,19-21,57</sup> only when the Co core and CoO shell have similar dimensions. By appealing to neutron diffraction measurements carried out on similar nanoparticles, we argue that the core and shell are over-coupled when the CoO shell is thin, locking the shell moments to the reorienting core. Conversely, when the CoO shell is much thicker than the core radius, the shell is under coupled, and we regain the same dynamics expected for bare Co particles. Only when there is a CoO shell, which is sufficiently thick to have both a moment-bearing layer at the interface for core-shell coupling and a substantial volume with the moment compensated bulk CoO structure can we expect to see a substantial exchange bias effect.

## ACKNOWLEDGMENTS

We are grateful to L. Yang for helping with the SAXS experiments. We also acknowledge S. Kline for helping with the SAXS data analysis. This work was carried out under the auspices of the U.S. Department of Energy, Office of Basic Energy Sciences at Brookhaven National Laboratory under Contract No. DE-AC02-98CH1886. Use of the National Synchrotron Light Source, Brookhaven National Laboratory, was supported by the U.S. Department of Energy, Office of Science, Office of Basic Energy Sciences, under Contract No. DE-AC02-98CH10886.

\*maronson@bnl.gov

<sup>1</sup>W. H. Meiklejohn, *J. Appl. Phys.* **33**, 1328 (1962).

<sup>2</sup>J. Nogués, J. Sort, V. Langlais, V. Skumryev, S. Suriñach, J. S. Muñoz, and M. D. Baró, *Phys. Rep.* **422**, 65 (2005).

<sup>3</sup>J. Nogués and I. K. Schuller, *J. Magn. Magn. Mater.* **192**, 203 (1999).

<sup>4</sup>V. Skumryev, S. Stoyanov, Y. Zhang, G. Hadjipanayis, D. Givord, and J. Nogués, *Nature (London)* **423**, 850 (2003).

<sup>5</sup>A. E. Berkowitz and K. Takano, *J. Magn. Magn. Mater.* **200**, 552 (1999).

<sup>6</sup>L. Smardz, U. Köbler, and W. Zinn, *Vacuum* **42**, 283 (1991).

<sup>7</sup>F. Radu, M. Etzkorn, R. Siebrecht, T. Schmitte, K. Westerholt, and H. Zabel, *Phys. Rev. B* **67**, 134409 (2003).

<sup>8</sup>M. Gruyters and D. Riegel, *Phys. Rev. B* **63**, 052401 (2000).

<sup>9</sup>M. D. Stiles and R. D. McMichael, *Phys. Rev. B* **63**, 064405 (2001).

<sup>10</sup>M. Kiwi, *J. Magn. Magn. Mater.* **234**, 584 (2001).

<sup>11</sup>P. J. van der Zaag, A. R. Ball, L. F. Feiner, R. M. Wolf, and P. A. A. van der Heijden, *J. Appl. Phys.* **79**, 5103 (1996).

<sup>12</sup>T. Lin, C. Tsang, R. E. Fontana, and J. K. Howard, *IEEE Trans. Magn.* **31**, 2585 (1995).

<sup>13</sup>M. Ali, C. H. Marrows, M. Al-Jawad, B. J. Hickey, A. Misra, U. Nowak, and K. D. Usadel, *Phys. Rev. B* **68**, 214420 (2003).

<sup>14</sup>V. Baltz, J. Sort, S. Landis, B. Rodmacq, and B. Dieny, *Phys. Rev. Lett.* **94**, 117201 (2005).

<sup>15</sup>S. Gangopadhyay, G. C. Hadjipanayis, C. M. Sorensen, and K. J.

- Klabunde, *J. Appl. Phys.* **73**, 6964 (1993).
- <sup>16</sup>M. Kovylyna, M. García del Muro, Z. Konstantinović, M. Varela, O. Iglesias, A. Labarta, and X. Batlle, *Nanotechnology* **20**, 175702 (2009).
- <sup>17</sup>B. Beschoten, J. Keller, P. Miltényi, and G. Güntherodt, *J. Magn. Magn. Mater.* **240**, 248 (2002).
- <sup>18</sup>V. P. Nascimento, E. C. Passamani, A. D. Alvarenga, A. Biondo, F. Pelegrini, and E. Baggio Saitovitch, *Appl. Surf. Sci.* **254**, 2114 (2008).
- <sup>19</sup>S. E. Inderhees, J. A. Borchers, K. S. Green, M. S. Kim, K. Sun, G. L. Strycker, and M. C. Aronson, *Phys. Rev. Lett.* **101**, 117202 (2008).
- <sup>20</sup>J. B. Tracy, D. N. Weiss, D. P. Dinega, and M. G. Bawendi, *Phys. Rev. B* **72**, 064404 (2005).
- <sup>21</sup>G. Salazar-Alvarez, J. Sort, S. Suriñach, M. D. Baró, and J. Nogués, *J. Am. Chem. Soc.* **129**, 9102 (2007).
- <sup>22</sup>S. Sako, K. Ohshima, and M. Sakai, *J. Phys. Soc. Jpn.* **70**, 2134 (2001).
- <sup>23</sup>V. F. Puentes, K. M. Krishnan, and A. P. Alivisatos, *Science* **291**, 2115 (2001).
- <sup>24</sup>M. Gierlings, M. J. Prandolini, H. Fritzsche, M. Gruyters, and D. Riegel, *Phys. Rev. B* **65**, 092407 (2002).
- <sup>25</sup>J. Keller, P. Miltényi, B. Beschoten, G. Güntherodt, U. Nowak, and K. D. Usadel, *Phys. Rev. B* **66**, 014431 (2002).
- <sup>26</sup>S. G. E. te Velthuis, A. Berger, G. P. Felcher, B. K. Hill, and E. Dan Dahlberg, *J. Appl. Phys.* **87**, 5046 (2000).
- <sup>27</sup>J. Nogués, C. Leighton, and I. K. Schuller, *Phys. Rev. B* **61**, 1315 (2000).
- <sup>28</sup>R. K. Zheng, G. H. Wen, K. K. Fung, and X. X. Zhang, *J. Appl. Phys.* **95**, 5244 (2004).
- <sup>29</sup>E. P. Wohlfarth, *Ferromagnetic Materials* (North-Holland, Amsterdam, 1980).
- <sup>30</sup>R. H. Kodama, *J. Magn. Magn. Mater.* **200**, 359 (1999).
- <sup>31</sup>J. Nogués, V. Skumryev, J. Sort, S. Stoyanov, and D. Givord, *Phys. Rev. Lett.* **97**, 157203 (2006).
- <sup>32</sup>D. Peddis, S. Laureti, M. V. Mansilla, E. Agostinelli, G. Varvaro, C. Cannas, and D. Fiorani, *Superlattices Microstruct.* **46**, 125 (2009).
- <sup>33</sup>M. Vasilakaki, E. Eftaxias, and K. N. Trohidou, *Phys. Status Solidi* **205**, 1865 (2008).
- <sup>34</sup>S. R. Kline, *J. Appl. Crystallogr.* **39**, 895 (2006).
- <sup>35</sup>P. Bartlett and R. H. Ottewill, *J. Chem. Phys.* **96**, 3306 (1992).
- <sup>36</sup>M. Bonini, E. Fratini, and P. Baglioni, *Mater. Sci. Eng., C* **27**, 1377 (2007).
- <sup>37</sup><http://www.ncnr.nist.gov/resources/sldcalc.html>.
- <sup>38</sup>A. Wiedenmann, *Physica B* **356**, 246 (2005).
- <sup>39</sup>A. Wiedenmann, *J. Appl. Crystallogr.* **33**, 428 (2000).
- <sup>40</sup>A. N. Dobrynin, A. K. Temst, P. Lievens, J. Margueritat, A. J. Gonzalo, C. N. Afonso, E. Piscopiello, and G. Van Tendeloo, *J. Appl. Phys.* **101**, 113913 (2007).
- <sup>41</sup>D. Le Messurier, R. Wintera, and C. M. Martin, *J. Appl. Crystallogr.* **39**, 589 (2006).
- <sup>42</sup>C. Neto, M. Bonini, and P. Baglioni, *Colloids Surf., A* **269**, 96 (2005).
- <sup>43</sup>D. L. Leslie-Pelecky and R. D. Rieke, *Chem. Mater.* **8**, 1770 (1996).
- <sup>44</sup>M. S. Lund, W. A. A. Macedo, K. Liu, J. Nogués, I. K. Schuller, and C. Leighton, *Phys. Rev. B* **66**, 054422 (2002).
- <sup>45</sup>A. N. Dobrynin, D. N. Ievlev, K. Temst, P. Lievens, J. Margueritat, J. Gonzalo, C. N. Afonso, S. Q. Zhou, and A. Vantomme, *Appl. Phys. Lett.* **87**, 012501 (2005).
- <sup>46</sup>D. L. Peng, K. Sumiyama, T. Hihara, S. Yamamuro, and T. J. Konno, *Phys. Rev. B* **61**, 3103 (2000).
- <sup>47</sup>T. Ambrose and C. L. Chien, *Phys. Rev. Lett.* **76**, 1743 (1996).
- <sup>48</sup>P. J. van der Zaag, Y. Ijiri, J. A. Borchers, L. F. Feiner, R. M. Wolf, J. M. Gaines, R. W. Erwin, and M. A. Verheijen, *Phys. Rev. Lett.* **84**, 6102 (2000).
- <sup>49</sup>U. Nowak, K. D. Usadel, J. Keller, P. Miltényi, B. Beschoten, and G. Güntherodt, *Phys. Rev. B* **66**, 014430 (2002).
- <sup>50</sup>C. G. Shull, W. A. Strauser, and E. O. Wollan, *Phys. Rev.* **83**, 333 (1951).
- <sup>51</sup>W. L. Roth, *Phys. Rev.* **110**, 1333 (1958).
- <sup>52</sup>B. van Laar, *Phys. Rev.* **138**, A584 (1965).
- <sup>53</sup>W. Jauch, M. Reehuis, H. J. Bleif, F. Kubanek, and P. Pattison, *Phys. Rev. B* **64**, 052102 (2001).
- <sup>54</sup>K. Takano, R. H. Kodama, A. E. Berkowitz, W. Cao, and G. Thomas, *Phys. Rev. Lett.* **79**, 1130 (1997).
- <sup>55</sup>R. Jungblut, R. Coehoorn, M. T. Johnson, J. aan de Stegge, and A. Reinders, *J. Appl. Phys.* **75**, 6659 (1994).
- <sup>56</sup>N. J. Gokemeijer, R. L. Penn, D. R. Veblen, and C. L. Chien, *Phys. Rev. B* **63**, 174422 (2001).
- <sup>57</sup>W. J. Meiklejohn and C. P. Bean, *Phys. Rev.* **102**, 1413 (1956).